Applied Mathematics & Information Sciences
An International Journal

http://dx.doi.org/10.18576/amis/170419

Numerical Design and Optimization of Near-Infrared Band-Pass Filter

Hafiza Syeeda Faiza[1], *Ghazi Aman Nowsherwan*[1], *Basem Abu Izneid*[2], , *Muhammad Azhar*[1], *Saira Riaz*[1], *Syed Sajjad Hussain*[1,*], *Saira Ikram*[1], *Mohsin Khan*[1], *and Shahzad Naseem*[1], *Mohammad Kanan* [3], *and Ibrahim M. Mansour* [4]

[1]Centre of Excellence in Solid State Physics, University of the Punjab, Lahore, 54590, Pakistan
[2] Department of Electrical Engineering, College of Engineering, University of Business and Technology, 21448, Saudi Arabia
[3] Department of Industrial Engineering, College of Engineering, University of Business and Technology, 21448, Saudi Arabia
[4] Electrical Department Faculty of Engineering Zarqa University, Zarqa, Jordan

Received: 22 Jan. 2023, Revised: 22 Feb. 2023, Accepted: 22 Mar. 2023
Published online: 1 Jul. 2023

Abstract: Band-pass filters functioning in the near-infrared (IR) range are desired for laser technology, multi-photon fluorescence, and IR imaging applications. In this study, we have designed four band-pass filters in the near Infrared spectrum (900-1200 nm) by vertically stacking different high and low-index materials. The band-pass filters are modelled by Essential Macleod software with different thicknesses. The layer's thicknesses were optimized in such a way to provide negligible reflectance and maximum transmission on the front side. All the simulated band-pass filters exhibit high transmittance, but TiO2/Al2O3 and Ta2O5/Al2O3 outperforms other modelled structure in terms of performance due to the better incorporation of high and low-index material. Furthermore, we have also investigated the effect of different substrates. Out of all substrates, glass, and ITO substrates performed well because their refractive index is in close proximity to the requirements to get minimum reflectance. These findings point to a viable future approach for optical band-pass filters operating in the infrared spectrum.

Keywords: Optical filters, Infrared spectrum, simulation, band pass filters, refractive index.

1 Introduction

Optical band-pass filters (OBF) selectively transmit distinct wavelengths and are essential for sensing, imaging systems, spectroscopy, phototherapy, and laser surgery, according to [1-6]. Researchers have focused on emerging materials used for optical coatings and filters that operate mainly in the infrared (IR) region over the last decade, as the IR based optical coatings are very valuable in an extensive range of technological applications, including IR spectroscopy, laser technology, multi-photon fluorescence, IR imaging, thermography, automatic protection, and astrometry [7-10]. Computer-assisted models for developing and upgrading OBFs with pinpoint perfection assist in these efforts. Tunable optical properties are significant for optimizing the available observable information [11, 12]. The essential aspects in influencing the overall performance of OBFs are the refractive index, thickness, and material selection for the needed application.

Recent research has shown that different stacks of thin films with an optimal mix of interface reflectance losses and refractive indices may be used to create and regulate the spectrum frequency of optical signals for a variety of applications [13-15]. Low and high-refractive-index (nL and nH) layers are finely controlled in OBFs to manage light intensity and wavelength range [16]. Siliva, M. et al. simulated two Fabry-Perot thin-film resonators made of (TiO_2) and (SiO_2) attached to the top of an LED for endoscope imaging diagnosis. At central wavelengths of 415 nm and 436 nm, they observed the blue and green LEDs connected with the Fabry-Perot resonator had the highest spectrum transmittance of 21% and 33%, respectively [17]. H. Yoda et al. investigated the optical properties of a-Si:H/SiO_2 multi-layer films prepared by RF sputtering for optical band-pass filters (OBFs). They discovered a refractive index of 3.6 and an extinction coefficient of less than 10^{-4} by immersing low refractive index material in high index refractive index material [18]. X. Wang et al. created TiO_2–SiO_2 composite coatings on Si wafers and glass substrates using plasma sputtering. Compared to a glass substrate, they observed that composite films on Si substrate had a transmittance of more than 90% [19]. S. Zaitsu et al. created multi-layers of titania and alumina using atomic layer deposition (ALD). They observed a significant shift in refractive index as titania thickness rose from 2 to 39 Aº [20]. M. Kumar et al. entails

*Corresponding author E-mail: sajjadh.cssp@pu.edu.pk

the deposition and optical characterization of five stacked multi-layer structures of TiO_2-Al_2O_3 and TiO_2-SiO_2 with varying thicknesses for distinct wavelength ranges in the visible area. Their findings demonstrated a 70–75 % reflectivity and a huge reflection band [21]. J. Liu et al. used e-beam evaporation to create single-layer films of Al_2O_3 and TiO_2 onto glass substrates for broadband Bragg-reflecting blue light coatings. Their composite displayed good transparency within a single period, and Bragg's reflection became visible as the period increased [22]. A. Szeghalmi et al. used ALD to make alumina and titania hetero-layer thin films on various substrates and looked at how temperature affected the refractive index. The refractive index of titania grows dramatically as temperature rises, but the refractive index of Al_2O3 is unaffected by temperature since it is temperature sensitive [23]. When X. Liu et al. used ALD to create a notch filter, they found that the average reflectance in 510-590 nm wavelength region was 86.7 %, which was very close to the experimental data [24]. N. Anwar used hetero-layers of TiO_2/Al_2O_3 with various combinations of layers to create and simulate the band-pass and edge filter filters. A 7-layer longwave pass edge filter achieved a transmission of 54.60 % and a 14-layer band-pass filter yields a reflectance of 15% in their model. [25]. The utilization of different lustrous elements such as gold (Au), silver (Ag), and rare earth elements, as well as sophisticated manufacturing procedures, have been reported to operate OBFs in the visible area of the spectrum [26-28].

In this study, we designed several optical band-pass (OBP) filters as $[HL]^5$ H using half-wave and quarter-wave stacks of regularly repeating high and low-index materials. The band-pass area was designed to transmit a specific range of wavelengths from 900 nm to 1200 nm. Our modeled OBFs have good transmission in the near IR region and are beneficial for building superior band-pass filters in the infrared spectrum for applications like laser technology, multi-photon fluorescence, and IR imaging.

2 Optical Filter Design and Simulation details

2.1 Approach and Methodology

Essential Macleod is a tool for developing and estimating the performance of optical coatings. Macloed's standard approach for computing the characteristics of optical coatings moves the overall electric field and magnetic field parallels to each interface from the back to the front of the assembly [29, 30]. Every film is depicted as a transfer matrix, and the electric and magnetic fields are represented as column vectors. As a result, the multiplication of the column vectors by the transfer matrix in order is required for the computation. It is common practice to normalize the electromagnetic field amplitudes such that their amplitudes are equal at the final interface. The letters B and C commonly denote the normalized electromagnetic field at the multi-layers entry. These equations are expressed mathematically as follows;

$$\begin{bmatrix} B \\ C \end{bmatrix} = \left\{ \prod_{j=1}^{q} \begin{bmatrix} \cos\delta_j & \frac{i\sin\delta_j}{\eta_j} \\ i\eta_j \sin\delta_j & \cos\delta_j \end{bmatrix} \right\} \begin{bmatrix} 1 \\ \eta_{sub} \end{bmatrix} \quad (1)$$

and reflectance and transmittance can be calculated from the relations,

$$R = \frac{(\eta_0 B - C)(\eta_0 B - C)^*}{(\eta_0 B + C)(\eta_0 B + C)^*} \quad (2)$$

And,

$$T = \frac{4\eta_0 \text{Real}\,(\eta_{sub})}{(\eta_0 B + C)(\eta_0 B + C)^*} \quad (3)$$

2.2. Concept and Design of OBF

A single spacer (resonant cavity) is placed between two multi-layer dielectric mirrors in the simplest thin-film optical band-pass filters. [30-33]. DBRs (Distributed Bragg Reflectors) are dielectric mirrors that produce a spectrum rejection region by alternating high and low-index materials with several layers. The reflection minimum is reached at a certain (central) wavelength when the optical thickness is a one-fourth of the incoming wavelength. An embedded spacer creates a transmission passband, and its optical thickness dictates the central or reference wavelength (CWL) of the filter.

In this investigation, we designed four band-pass filters in the IR range with different combinations of high and low index materials. The Essential Macleod software tests the simulation of a hetero-layers stack of alternate layers of thin films. The band-pass filter was made of air, $[HL]^5$ H, glass, as indicated in Fig. 1, where “H” corresponds to high index materials (TiO_2, Ta_2O_5) and “L” corresponds to low index material (Al_2O_3, Y_2O_3). The profile of the hetero-layer stack's refractive index as a function of thickness may be seen in Fig. 2, which depicts the profile in the z-direction. At a specific wavelength, the layers of TiO_2 and Ta_2O_5, which had a refractive index of 2.25 and 2.11, respectively, served as the high index layer (nH), while the layers of Al_2O_3 and Y_2O_3, which had a refractive index of 1.65 and 1.77, served as the low index layer (nL). In the 11-layer band-pass filter, the thickness of each layer was determined by using the half-wave and quarter-wave stack designs, respectively. The design utilized high index materials (TiO_2 and Ta_2O_5) as the front and back layers. Each layer with a high index has a thickness equal to half a wave, whereas each layer with a low index has a thickness equal to one-quarter of a wave. Table 1 lists the possible combinations of high-index and low-index materials, as well as the thickness of each of the 11 layers that make up the band-pass filter in the near IR range. It is anticipated

that the entire thickness of the hetero-layer optical band-pass filter will be less than 2000 nm.

2.3. Software Model Validation

The Essential Macleod program includes all of the main features for creating optical coatings and assessing their performance. This software can test a wide range of output characteristics of a specific type of coating, including typical transmission and reflectance, ellipsometric values, ultrafast color, and as a function of wavelength from zero to the third derivative. With the help of this tool, we may also tweak current designs to improve their efficiency. The presented literature backs up the validity of Essential Macleod software verification [34-39], which contrasts coating performance based on real-world experimental characterization with theoretical findings generated by the software. As a result, it may validate the feasibility and availability of device configurations and material values within a particular scope.

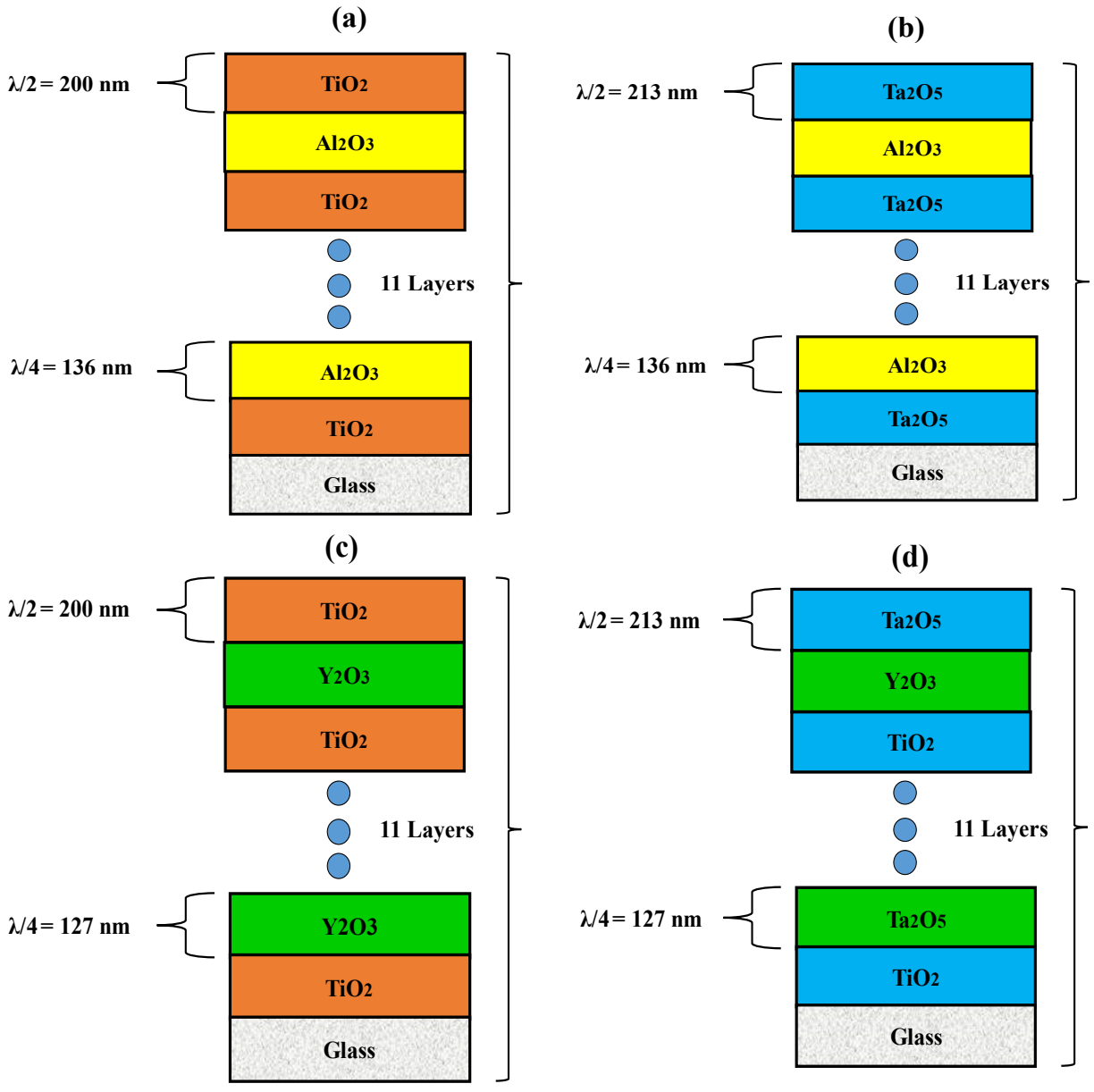

Fig. 1: (a) Physical design of 11 layer stack $[TiO_2\ Al_2O_3]^5\ TiO_2$ on glass substrate, (b) Physical design of 11 layer stack of $[Ta_2O_5\ Al_2O_3]^5\ Ta_2O_5$ on glass substrate, (c) Physical design of 11 layer stack of $[TiO_2\ Y_2O_3]^5\ TiO_2$ on glass substrate, and (d) Physical design of 11 layer stack of $[Ta_2O_5\ Y_2O_3]^5\ Ta_2O_5$ on glass substrate.

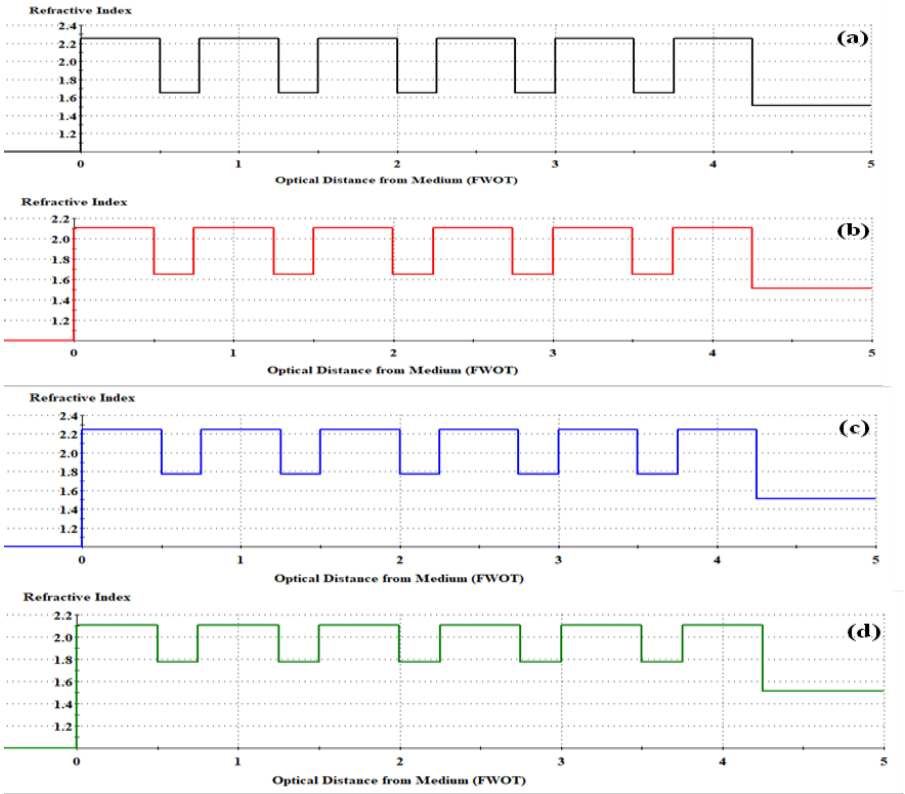

Fig. 2: (a,b,c,d) Change in the refractive index versus optical distance from the medium (FWOT) of 11 layer stack of $[TiO_2\ Al_2O_3]^5$ TiO_2 , $[Ta_2O_5\ Al_2O_3]^5$ Ta_2O_5 , $[TiO_2\ Y_2O_3]^5$ TiO_2 , and $[Ta_2O_5\ Y_2O_3]^5$ Ta_2O_5.

Table 1: Simulated design of modeled band-pass filter at reference wavelength of 900 nm.

Layer	Material	Physical Thickness (nm)	Material	Physical Thickness (nm)	Material	Physical Thickness (nm)	Material	Physical Thickness (nm)
Medium	Air		Air		Air		Air	
1	TiO_2	200.00	Ta_2O_5	213.36	TiO_2	200.00	Ta_2O_5	213.36
2	Al_2O_3	136.29	Al_2O_3	136.29	Y_2O_3	126.90	Y_2O_3	126.90
3	TiO_2	200.00	Ta_2O_5	213.36	TiO_2	200.00	Ta_2O_5	213.36
4	Al_2O_3	136.29	Al_2O_3	136.29	Y_2O_3	126.90	Y_2O_3	126.90
5	TiO_2	200.00	Ta_2O_5	213.36	TiO_2	200.00	Ta_2O_5	213.36
6	Al_2O_3	136.29	Al_2O_3	136.29	Y_2O_3	126.90	Y_2O_3	126.90
7	TiO_2	200.00	Ta_2O_5	213.36	TiO_2	200.00	Ta_2O_5	213.36
8	Al_2O_3	136.29	Al_2O_3	136.29	Y_2O_3	126.90	Y_2O_3	126.90
9	TiO_2	200.00	Ta_2O_5	213.36	TiO_2	200.00	Ta_2O_5	213.36
10	Al_2O_3	136.29	Al_2O_3	136.29	Y_2O_3	126.90	Y_2O_3	126.90
11	TiO_2	200.00	Ta_2O_5	213.36	TiO_2	200.00	Ta_2O_5	213.36
Substrate	Glass		Glass		Glass		Glass	
		1881.45		1961.62		1834.52		1914.69

3 Results and Discussion

3.1 Transmission and Reflection Spectra

In this kind of investigation, four band-pass filters are constructed in the near IR range with different high and low-index materials deposited one over the other, forming a series of cavity structures. Fig. 3 illustrates the obtained transmission and reflection spectra at a central wavelength of 900 nm. The pass region was designed to be from 700 nm to 1200 nm. To characterize the optical qualities, the complex-refractive index n(λ) is stated in the equation [38]

$$n(\lambda) = n_l + ik \qquad (4)$$

where "n" is a real part of the refractive index, and "k" is the imaginary part of the complex-refractive index representing the extinction coefficient. In absorption-free layers, n(λ) = 0= 0, but in semiconductors and metals, the value will be larger when absorption is greater. To achieve the overall effectiveness of an optical band-pass filter, the layer thickness must be optimized to provide the least absorbance on the front side. The condition to get minimum reflectance is expressed in the equation.

$$d = \frac{\lambda}{4n_1} + m\frac{\lambda}{2n_1}(m = 0,1,2,3\ldots) \qquad (5)$$

The band must be placed in the correct region, which might be difficult to do with a single layer of coating. It is possible to reduce the amount of reflection produced by optical filters with many layers by adjusting the thickness of each layer following the parameters of a quarter-wavelength. It is advised that the thickness of the coating layers be about equal to a quarter or a half wavelength of the incoming light. To achieve destructive interference, the magnitudes of the reflecting beams at the air-coating boundary and the substrate-coating boundary must be equal in order for them to be exactly half out of phase with one another. [38, 40, 41]. Another way to get the minimum reflectance is by carefully picking a material that satisfies the following relation, where n_s and n_o is the refractive index of substrate and air.

$$n_1 = \sqrt{n_s n_o} \qquad (6)$$

Herein, the optical thickness of high index material in a stack is taken as twice of a quarter wavelength. In contrast, the optical thickness of low-index material in a stack is set as a quarter wavelength. The formula employed for the band-pass filter was $[HL]^5$ H, so the target specification could be limited to the pass region. It can be visualized from Fig. 3, that with the increase in wavelength, transmission increases, and reflection decreases from 700 nm. All the designed filter exhibits high performance. But the utmost transmission of 99.14% and minimum reflection of 0.84 % was observed at 1160 nm in the case of Ta_2O_5/Al_2O_3 due to better incorporation of high index and low index material. After 1200 nm, transmission decreases, and reflections increase.

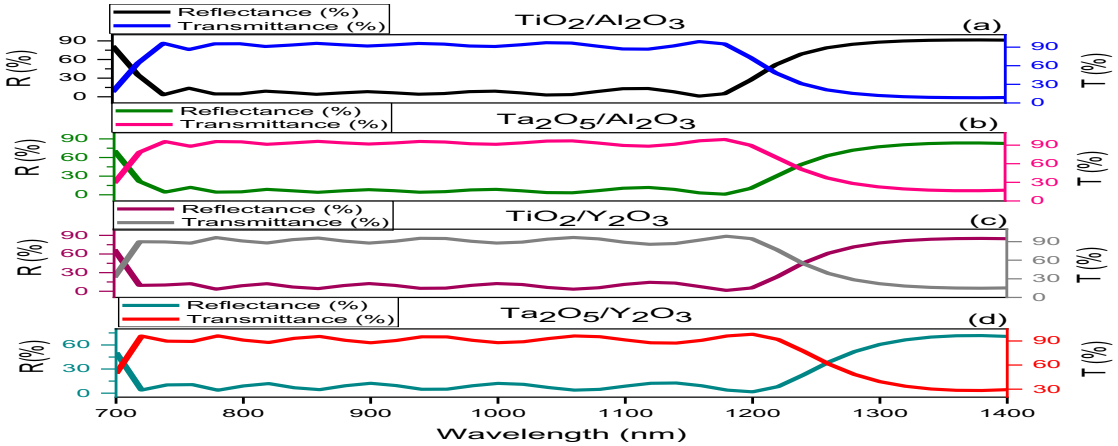

Fig. 3: (a,b,c,d) Transmission (%) and reflectance (%) spectra versus wavelength (nm) in the IR spectrum of optical band-pass filter of $[TiO_2\ Al_2O_3]^5\ TiO_2$, $[Ta_2O_5\ Al_2O_3]^5\ Ta_2O_5$, $[TiO_2\ Y_2O_3]^5\ TiO_2$, and $[Ta_2O_5\ Y_2O_3]^5\ Ta_2O_5$.

3.2. 3 D plot of Transmission and Reflection

The relation between parameters; wavelength, incident angle, transmittance, and reflection is given by 3D plot. It is a handy tool in MacLeod software to analyze the relationship between these quantities. Fig. 4 and Fig. 5 illustrate the transmission and reflection magnitude and mean polarization over the range of 900 nm to 1400 nm and angle of incidence 0° to 80°. It can be depicted from Fig. 4 and Fig. 5 that with increasing wavelength and incident angle, the transmission increases and reflection decrease in the near IR region. However, the transmission falls for the high value of wavelength, i.e. mid-IR part.

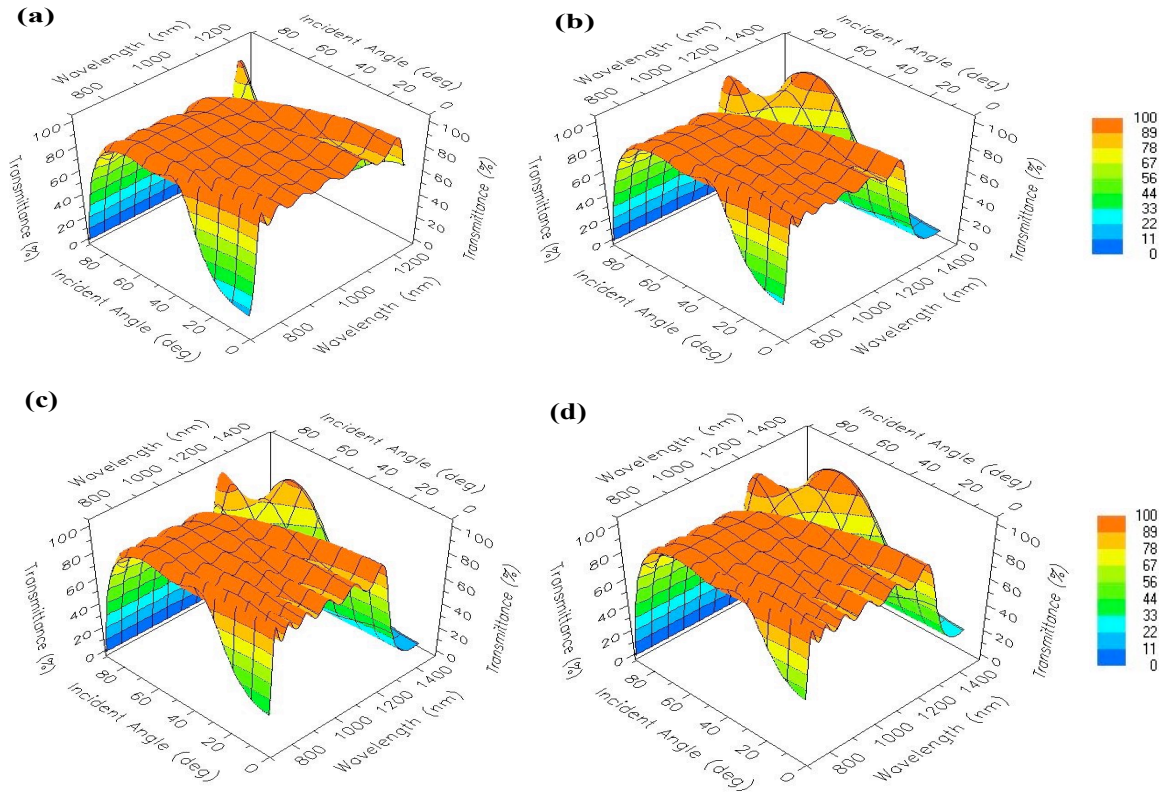

Fig. 4: (a,b,c,d) 3D shape of transmission (%) spectra versus wavelength (nm) with angle of incidence (deg) of $[TiO_2\ Al_2O_3]^5\ TiO_2$, $[Ta_2O_5\ Al_2O_3]^5\ Ta_2O_5$, $[TiO_2\ Y_2O_3]^5\ TiO_2$, and $[Ta_2O_5\ Y_2O_3]^5\ Ta_2O_5$.

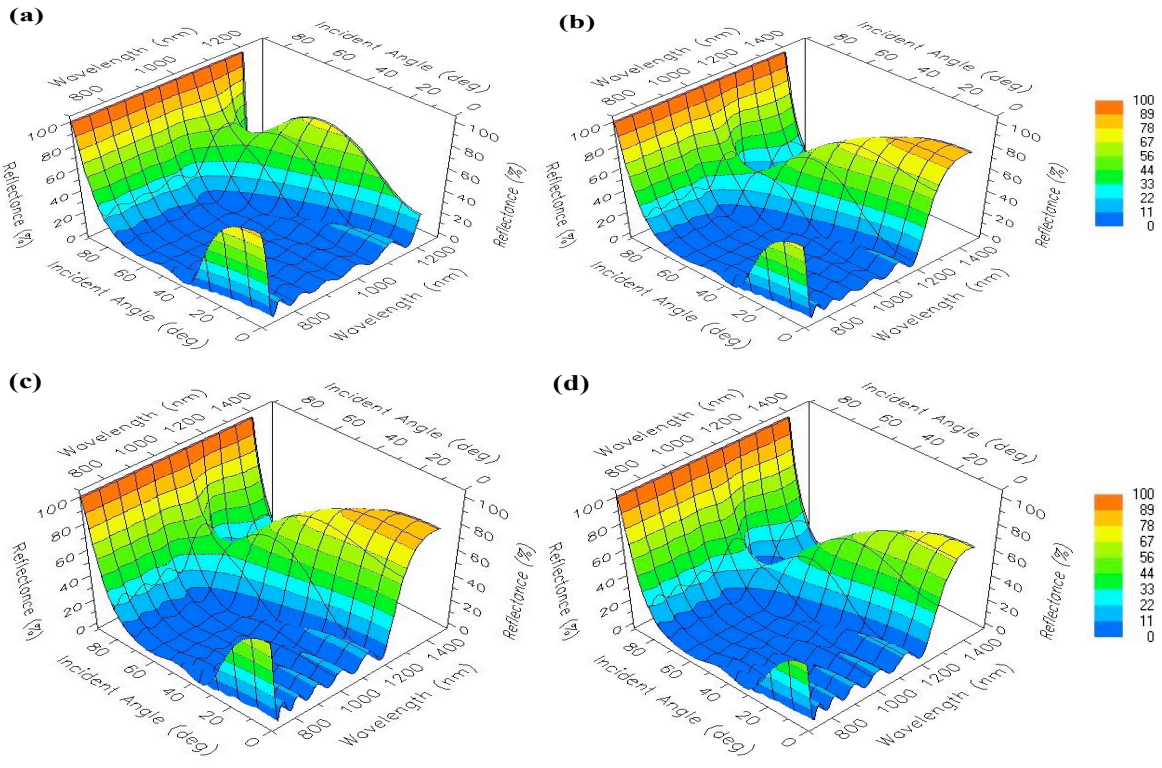

Fig. 5: (a,b,c,d) 3D shape of transmission (%) spectra versus wavelength (nm) with angle of incidence (deg) of $[TiO_2\ Al_2O_3]^5\ TiO_2$, $[Ta_2O_5\ Al_2O_3]^5\ Ta_2O_5$, $[TiO_2\ Y_2O_3]^5\ TiO_2$, and $[Ta_2O_5\ Y_2O_3]^5\ Ta_2O_5$.

3.3. Admittance Plot of designed filters

Admittance is the property of an optical material to accept or pass through specific wavelengths. The ratio of the magnetic field to the electric field may be regarded as the optical admittance. Due to the continuity criteria that exist on tangential electric and magnetic fields at any boundary, the record of the surface admittance will be a continuous one. Fig. 6 depicts the admittance diagram for our many design iterations. It is a graphical depiction of the math that was done to determine the qualities of the coating. It can be challenging, if not impossible, to track down the whole admittance diagram of the coating because the loci of a complex coating sometimes sit on top of one another. Thus, selecting a limited range of layers is thinkable for plotting. It does not change the locus of any layer. It is just that the layer outer the coverage does not have their loci plotted. All the designs show different admittance circles for high and low index material. It can be depicted that the locus of high index material doesn't reach point 1.0 on the real axis where the reflectance is zero.

3.4. Density of designed filters

The density of the material generally relates to its physical thickness. When the density of an optical substance is high, it indicates that it is a good reflector. Similarly, if the density value is low, the optical substance is a suitable transmitter. The density plot of our designed filters is illustrated in Fig. 7. This indicates that the low density regime in the near IR range results in a high transmittance in this region. Still, the density is high in the far-infrared region, resulting in a high reflectance in this region.

3.5. Effect of varying substrate on the performance of OBF

We also looked at the influence of different substrates on Ta_2O_5/Al_2O_3-based band-pass filter performance in this paper. One of the key factors that reduce the efficacy of optical coatings or filters is the suitable substrate. To achieve the minimum reflection of light with the substrate's help, the substrates' refractive index must be modified to get the lowest reflectance and highest transmission. The simulated data in Fig. 8 clearly shows considerable variations in the transmission and reflectance spectra when the refractive index of the substrate changes, which can be attributed to the substrate's optical characteristics like band-gap, refractive index, transparency and absorption coefficient. A substrate with the right refractive index value is required to obtain the lowest reflectance and thin film effects. In comparison to other substrates, glass and ITO perform well in the band-pass region because they match the standards and needs of optical coatings. Si and Ge, on the other hand, behave as semiconductors with a very high refractive index and a small band gap, resulting in absorption and reflection in the band-pass area, which restricts light transmission at the air/coating and coating/substrate interfaces, resulting in a drop in performance.

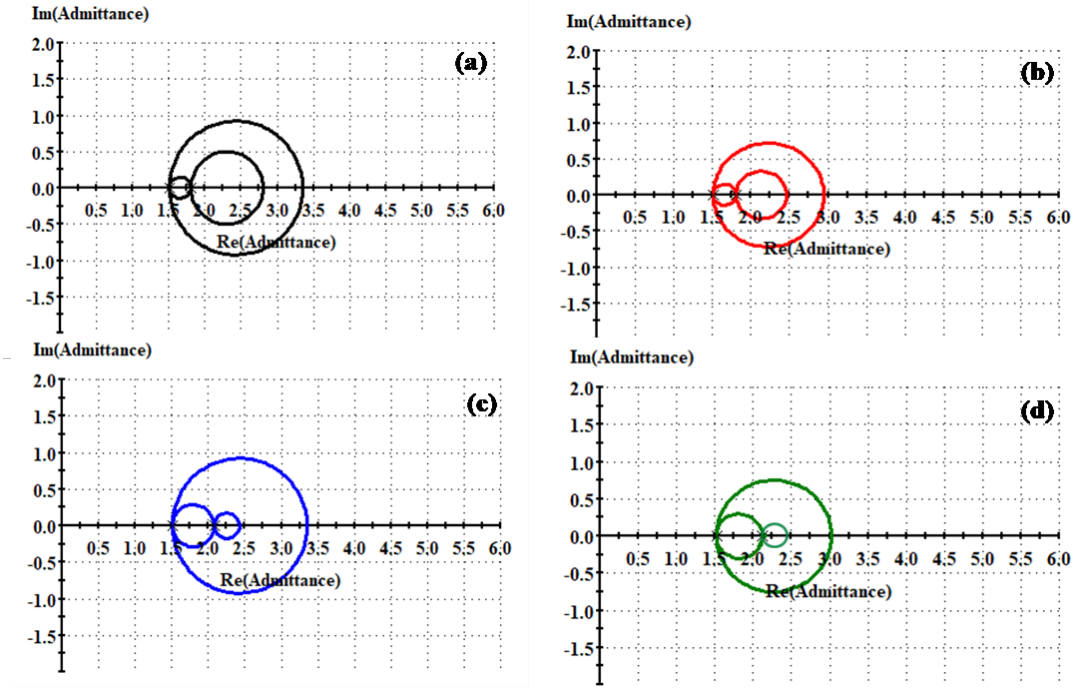

Fig. 6: (a,b,c,d) Admittance plot of OBF-based on TiO_2 and Al_2O_3 , Ta_2O_5 and Al_2O_3 , TiO_2 and Y_2O_3, and Ta_2O_5 and Y_2O_3.

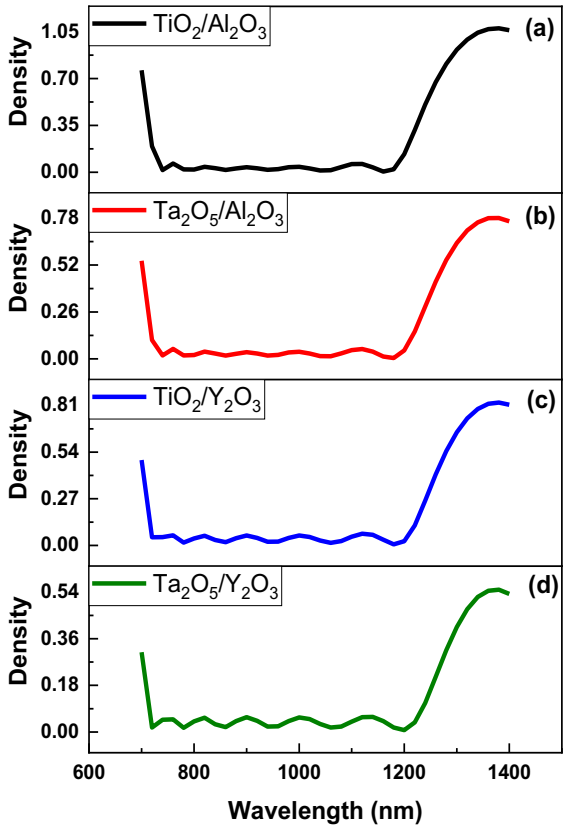

Fig. 7: (a,b,c,d) Density versus wavelength (nm) plot of OBF-based on TiO_2 and Al_2O_3 , Ta_2O_5 and Al_2O_3 , TiO_2 and Y_2O_3, and Ta_2O_5 and Y_2O_3.

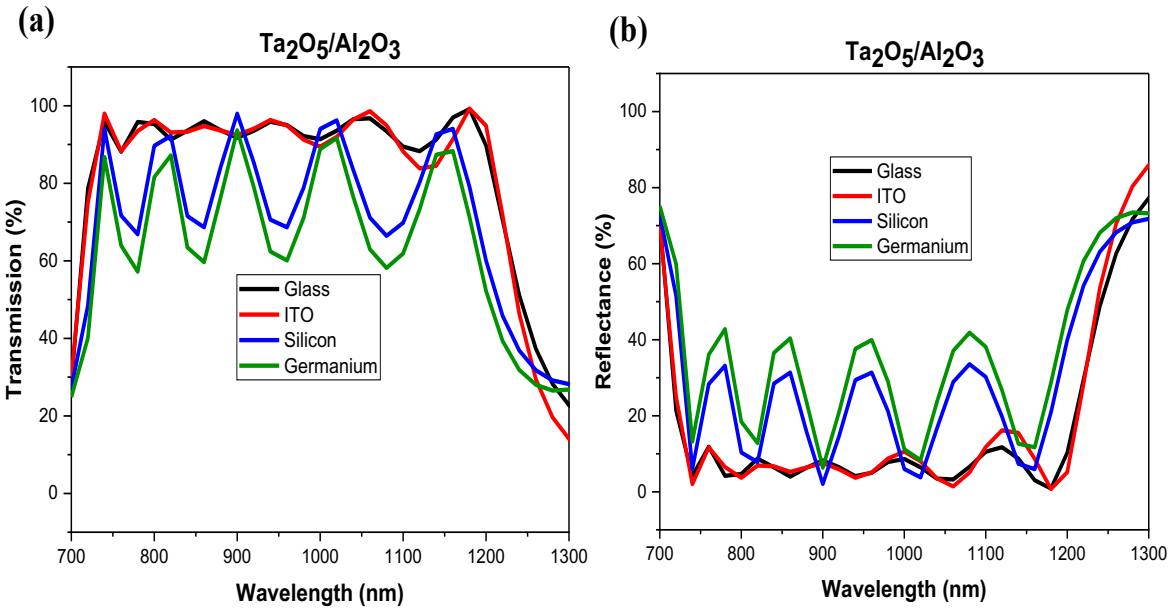

Fig. 8: (a) Transmission (%) spectra versus wavelength (nm) of different substrate in the IR spectrum of the optimized optical band-pass filter (b) Reflectance (%) spectra versus wavelength (nm) of different substrate of optimized optical band-pass filter.

4 Conclusions

In this investigation, four different optical band-pass filters were modelled and structured as $[H/L]^5$ H using Essential MacLeod software. The design and simulation analyses of the thin film layer were carried out using the basic theory of optical thin films in combination with the design software of the Essential Macleod film system. Glass was used as the substrate material at first, with TiO_2 and Ta_2O_5 serving as high-index materials (H) and Al_2O_3 and Y_2O_3 serving as low-index materials (L). It has been determined that all of the developed optical filters function well in the wavelength range of 900-1200 nm. However, due to the superior integration of high-index and low-index material, Ta_2O_5/Al_2O_3 had the highest transmission of 99.14 % and the lowest reflection of 0.84 % at 1160 nm. We've also looked at how different substrates affect the transmission and found that glass and ITO outperform other substrates. We concluded that optical-band filters can function better by carefully tweaking the settings. We believe that our designed band-pass filters give a potential future path for developing band-pass filters in the infrared spectrum with improved performance and suited for applications like laser technology, multi-photon fluorescence, and IR imaging.

Author contributions

All of the authors have acknowledged full responsibility for the presented manuscript's content and have authorized its submission.

Conflict of interest statement

The authors declare no conflicts of interest regarding this article.

References

[1] Haas, Julian, and B. Mizaikoff. Advances in mid-infrared spectroscopy for chemical analysis. *Annual Review of Analytical Chemistry*, **9**, 45-68 (2016).

[2] Liu, Changbo, Q. Zhang, D. Wang, G. Zhao, X. Cai, L. Li, H. Ding, High Performance, Biocompatible Dielectric Thin-Film Optical Filters Integrated with Flexible Substrates and Microscale Optoelectronic Devices, *Advanced Optical Materials*, **6**, 1800146 (2018).

[3] Mitra, Chayan. Mid-infrared spectroscopy and challenges in industrial environment. *Infrared Spectroscopy-Principles, Advances, and Applications*. (2019).

[4] T. Kaya, Sevgi, and C. W. Huck, A review of mid-infrared and near-infrared imaging: principles, concepts and applications in plant tissue analysis, *Molecules,* **22**, 168 (2017).

[5] Young, E., A. M.Innes, and M. Jindal, Lasers in stapes surgery: a review, *The Journal of Laryngology & Otology*, **129**, 627-633 (2015).

[6] Zharov, Vladimir P., Yulian A. Menyaev, V. A. Hamaev, G. M. Antropov, and M. Waner, Optoelectronic microdevices for combined phototherapy, *Micro-and Nanotechnology for Biomedical and Environmental Applications*, **3912**, 11-22 (2000).

[7] Bhargava, Rohit, Infrared spectroscopic imaging: the next generation, *Applied spectroscopy*, **66**, 1091-1120 (2012).

[8] Greene, Thomas P., Douglas M. Kelly, J. Stansberry, J. Leisenring, E. Egami, E. Schlawin, L. Chu, K.W. Hodapp, and M. Rieke, λ= 2.4 to 5 μm spectroscopy with the James Webb Space Telescope NIRCam instrument, *Journal of astronomical telescopes, instruments, and systems*, **3**, 035001-035001 (2017).

[9] Law, S., V. Podolskiy, and D.J.N, Towards nano-scale photonics with micro-scale photons: the opportunities and challenges of mid-infrared plasmonics, Wasserman, *Nanophotonics*, **2**, 103-130 (2013).

[10] Tattersall, G. J., Infrared thermography: A non-invasive window into thermal physiology, *Comparative Biochemistry and Physiology Part A: Molecular & Integrative Physiology*, **202**, 78-98 (2016).

[11] Gat, Nahum, Imaging spectroscopy using tunable filters: a review. *Wavelet Applications VII* ,**4056,** 50-64 (2000).

[12] Lapray, P. Jean, X. Wang, J-B Thomas, and P. Gouton, Multispectral filter arrays: Recent advances and practical implementation, *Sensors*, **14**, 21626-21659 (2014).

[13] Bhamare, S. D. *Determination of Optimal Material Combination for Multilayer Thin Films to Improve Performance Against Surface Crack Propagation* (Doctoral dissertation, University of Cincinnati), (2009).

[14] Kitui, M., M. M. Mwamburi, F. Gaitho, and C. M. Maghanga, Optical Properties of TiO_2 Based Multilayer Thin Films: Application to Optical Filters, *International Journal of Thin Film Science and Technology,* **4**, 1 (2015).

[15] Putz, Barbara, S. Wurster, T. E. J. Edwards, B. Völker, G. Milassin, D.M Többens, C. OA Semprimoschnig, and M. Jo Cordill, Mechanical and optical degradation of flexible optical solar reflectors during simulated low earth orbit thermal cycling. *Acta Astronautica***, 175**, 277-289 (2020).

[16] Matsumoto, Naoki, T. Nakagawa, K. Kageyama, N. Wada, and Y. Sakabe, Terahertz Band-Pass filter fabricated by multilayer ceramic technology, *Japanese journal of applied physics*, **45**, 7499 (2006).

[17] Silva, M. Fernando, and JA Tenreiro Machado, A literature review on the optimization of legged robots, *Journal of Vibration and Control*, **18**, 1753-1767 (2012).

[18] Yoda, Hidehiko, K. Shiraishi, Y. Hiratani, and O. Hanaizumi, a-Si: H/SiO_2 multilayer films fabricated by radio-frequency magnetron sputtering for optical filters, *Applied optics,* **43**, 3548-3554 (2004).

[19] Wang, Xinrong, et al.., Microstructure and optical properties of amorphous TiO_2-SiO_2 composite films synthesized by helicon plasma sputtering, *Thin solid films*, **338**, 105-109 (1999).

[20] Zaitsu, S. ichi, T. Jitsuno, M. Nakatsuka, T. Yamanaka, and S. Motokoshi. Optical thin films consisting of nanoscale laminated layers, *Applied physics letters,* **80**, 2442-2444 (2002).

[21] Kumar, M., Kumari, N., Rao, P. K., Karar, V., Ramagopal, S. V., & Sharma, A. L. (2015, June). Multi-layer dielectric thin-film optical filters for beam folding applications. In *International Conference on Optics and Photonics*, **9654,** 90-94 (2015).

[22] Liu, Jing, Chi-Yu Lin, Wen-Cheng Tzou, Nai-Kuei Hsueh, Cheng-Fu Yang, and Y. Chen. Reflection of Blue Light Using Bi-Layer Al_2O_3–TiO_2 E-Beam Coating Films, *Crystal Growth & Design*, **18**, 5426-5433 (2018).

[23] Szeghalmi, Adriana, M. Helgert, R. Brunner, F. Heyroth, U.

Gösele, and M. Knez, Atomic layer deposition of Al_2O_3 and TiO_2 multilayers for applications as bandpass filters and antireflection coatings, *Applied Optics,* **48**, 1727-1732 (2009).
[24] Li, Yanghui, W. Shen, X. Hao, T. Lang, S. Jin, and X. Liu, Rugate notch filter fabricated by atomic layer deposition, *Applied Optics,* **53**, 270-275 (2014).
[25] Anwar, Nadia, N. Hussain, S. Ao, S. Amjad, J. Arshad, T. Anwar, H. S Faiza, S.S Hussain, Tailoring TiO_2/Al_2O_3 heterolayers as optical filters for the visible region, *Nanoscale Advances,* **4**, 1608-1616 (2022).
[26] Jakšić, Zoran, M. Maksimović, and M. Sarajlić, Silver–silica transparent metal structures as bandpass filters for the ultraviolet range, *Journal of Optics A: Pure and Applied Optics* ,**7**, 51 (2004).
[27] Lou, Zaizhu, B. Huang, Z. Wang, Xiangchao Ma, R. Zhang, X. Zhang, X. Qin, Y. Dai, and M.H Whangbo, Ag6Si2O7: a silicate photocatalyst for the visible region, *Chemistry of Materials*, **26**, 3873-3875 (2014).
[28] Rahman, M.d Mobassar, A. Khaleque, M.T Rahman, and F. Rabbi, Gold-coated photonic crystal fiber-based polarization filter for dual communication windows, *Optics Communications*, **461**, (2020).
[29] Macleod, Angus, and C. Clark, Optical coating design with the Essential Macleod, (2012).
[30] Macleod, H. Angus, and H. A. Macleod. *Thin-film optical filters*, CRC press, (2010).
[31] Orfanidis, S. J., Electromagnetic waves and antennas, (2002).
[32] Piegari, Angela, and F. Flory, eds., *Optical thin films and coatings: From materials to applications,* Woodhead Publishing, (2018).
[33] Sarangan, Andrew., *Optical thin film design*, CRC Press, (2020).
[34] Awad, M. A., and A. H. Aly., Experimental and theoretical studies of hybrid multifunctional TiO_2/TiN/TiO_2, *Ceramics International*, **45**, 19036-19043 (2019).
[35] Cho, Yoonho, N.S. Parmar, S. Nahm, and J.W Choi, Essential Macleod Program (EMP) simulated fabrication of high-quality Zn: SnO_2/Ag/Zn: SnO_2 multilayer transparent conducting electrode on flexible substrates, *Ceramics International* **, 43**, 7216-7221 (2017).
[36] Hou, H. Gang, S. Hussain, H.C Shao, G.W Liu, M.S Wang, G.J Qiao, and A. Shaheen, Experimental insights on factors influencing sensitivity of thin film narrow band-pass filters, *Journal of Nanoelectronics and Optoelectronics***, 14**, 1548-1554 (2019).
[37] Su, Junhong, J. Chu, Q. Yu, and H. Jiang, Seventh Symposium on Novel Photoelectronic Detection Technology and Applications, **11763,** (2019).
[38] Simya, O. K., K. Balachander, D. Dhanalakshmi, and A. Ashok, Performance of different anti-reflection coating and TCO layers for kesterite based thin film photovoltaic devices using Essential Macleod simulation program, *Superlattices and Microstructure***, 145**, (2020).
[39] Zeng, H. Yuan, S. F. Tang, and T.C. Chen., Design and measurement of long-wavelength infrared antireflection coating multi-layers of SiO_2 and Si_3N_4 on silicon window by Macleod software and FTIR technique, *International Conference on Applied System Innovation* (ICASI), (2017).
[40] Priyadarshini, B. Geetha, and A. K. Sharma., Design of multi-layer anti-reflection coating for terrestrial solar panel glass, *Bulletin of Materials Science,* **39**, 683-689 (2016).
[41] Kaminski, Piotr, and M. Ziolek, Surface and catalytic properties of Ce-, Zr-, Au-, Cu-modified SBA-15. *Journal of Catalysism*, **312**, 249-262 (2014).